Journal of Geophysical Research: Space Physics

RESEARCH ARTICLE
10.1029/2018JA025680

Key Points:
- The influence of thermospheric effects of solar activity on traveling planetary-scale waves generated in the troposphere is simulated
- Changes in the zonal wind and temperature caused by solar activity variations can modify spatial distributions of the planetary-scale waves
- Solar activity variations can significantly (up to 100%) change amplitudes of waves coming to the thermosphere from below

Supporting Information:
- Supporting Information S1

Correspondence to:
A. V. Koval,
a.v.koval@spbu.ru

Citation:
Koval, A. V., Gavrilov, N. M., Pogoreltsev, A. I., & Shevchuk, N. O. (2018). Influence of solar activity on penetration of traveling planetary-scale waves from the troposphere into the thermosphere. *Journal of Geophysical Research: Space Physics*, *123*, 6888–6903. https://doi.org/10.1029/2018JA025680

Received 21 MAY 2018
Accepted 31 JUL 2018
Accepted article online 6 AUG 2018
Published online 22 AUG 2018

Influence of Solar Activity on Penetration of Traveling Planetary-Scale Waves From the Troposphere Into the Thermosphere

A. V. Koval[1], N. M. Gavrilov[1], A. I. Pogoreltsev[1,2], and N. O. Shevchuk[1]

[1]Department of Atmospheric Physics, Saint-Petersburg State University, St. Petersburg, Russia, [2]Department of Meteorological Forecasts, Russian State Hydrometeorological University, Saint-Petersburg, Russia

Abstract In this study, numerical simulations of planetary-scale waves (PSWs), generated in the troposphere, were performed for altitudes from the Earth's surface up to 300 km. The influence of thermospheric effects of solar activity (SA) on the amplitudes and phases of westward traveling PSWs with zonal wave numbers 1 and 2 and periods 4–16 days propagating from the troposphere was simulated. Such simulations for a large number of PSW modes in the thermosphere were made for the first time. The effects of SA changes at altitudes above 100 km were involved in the general circulation model MUAM. The ionospheric conductivities for minimum and maximum SA levels were included into the MUAM. The simulation results were averaged over two ensembles of model runs with different PSW phases for conditions corresponding to the high and low SA levels for January–February. PSW atmospheric refractivity index and Eliassen-Palm flux were calculated. They correspond to simulated changes in PSW amplitudes. Changes in the zonal velocity and temperature caused by the SA variations can modify spatial distributions of the westward traveling PSWs. Wave amplitudes significantly (up to 100%) decrease at the thermospheric heights under high SA, which is accompanied by decreasing vertical component of the Eliassen-Palm flux. The 7-, 10-, and 16-day PSWs could have larger partial reflection and worse propagation conditions than the 4- and 5-day waves in the Southern Hemisphere under the high SA. At altitudes below 100 km, minor differences in zonal velocity and PSW amplitudes between high and low SA are found.

1. Introduction

Planetary-scale waves (PSWs) in the atmosphere are global-scale oscillations in the thermosphere with periods of several days. These waves can be generated in the troposphere and stratosphere, and then they can propagate to the upper atmosphere. In the thermosphere, PSWs can produce frequently observed oscillations (e.g., Forbes et al., 2002; Forbes & Zhang, 2015; Pancheva et al., 2010). The main sources of PSWs could be topographic forcing, land-sea heating contrast, large-scale meteorological disturbances, etc. PSWs can contribute to the energy transfer between different atmospheric layers and play significant role in the formation of the general circulation of the middle and upper atmosphere (Holton, 1975). The interest in more accurate studies of the dynamical and thermal effects produced by PSWs at different atmospheric layers is constantly increasing.

Planetary-scale oscillations with identical or similar periods coexist regularly in the middle atmosphere and ionosphere (Chang et al., 2011; Pancheva & Mukhtarov, 2012). In particular, PSWs were detected during the analysis of observations of nighttime emissions at *F* layer heights (Takahashi et al., 2005). PSWs were also registered with Fabry-Perot spectrometer SATI (Lopez-Gonzalez et al., 2009) observing OH and O_2 emissions at altitudes 80–100 km. Registered PSWs were divided into the groups corresponding to 2-, 5-, 10-, and 16-day periods. Borries and Hoffmann (2010) showed the existence of strong planetary wave-type oscillations in the ionosphere by analyzing the maps of total electron content. They found that characteristics of standing and propagating waves in the ionosphere are similar to stratospheric planetary waves. Large-scale wave structures were detected from an analysis of the zonal variability of the nightglow hydroxyl emission (Zaragoza & Taylor, 2001) and from observations of thermospheric winds in the ionosphere by Fabry-Perot interferometers (Liu et al., 2014). Laštovicka (2006) assumed that planetary waves could propagate from the middle atmosphere to the ionospheric heights only indirectly, through secondary PSW excitation by dissipating planetary wave (PW) modulated tides (Meyer, 1999; Yamazaki & Richmond, 2013), or through

vertical plasma drifts (Liu & Richmond, 2013). At the same time, Takahashi et al. (2007) supposed that PSWs with periods of 3–4 days may propagate directly from the stratosphere to the heights of the ionosphere.

Numerical simulations of planetary waves having different periods and zonal wave numbers have been repeatedly performed. Among the recent studies, one should mention papers by Smith (2003), Liu et al. (2004), Akmaev (2011), Chang et al. (2014), Wang et al. (2017), etc. The global atmospheric circulation models extended to the ionospheric heights were also developed (e.g., Liu et al., 2018; Qian et al., 2013). Hoffmann and Jacobi (2006) found PSW manifestations at the midlatitude ionospheric heights of the Northern Hemisphere. They used maps of the total electron content obtained from the GPS and GLONASS satellites for the space weather forecasting. PSWs at ionospheric heights were also registered using the data of the ionosonde network at high latitudes of the Northern Hemisphere (Stray & Espy, 2018; Zhu et al., 2017).

Conditions of PSW generation and propagation may depend on cyclic changes of the solar activity (SA), for example, Geller and Alpert (1980) and Arnold and Robinson (1998). These changes can affect the temperature and circulation, and alter PSW propagation conditions by redistributing the incoming solar energy at various atmospheric layers (Chanin, 2006). Numerical simulations of SA effects on the temperature and zonal wind were performed by Krivolutsky et al. (2015) at altitudes up to 135 km and by Gan et al. (2017) in the mesosphere. Remote temperature measurements at mesopause altitudes showed the presence of PSWs with periods of 2–10 days, correlating with the 22-year *Hale cycle* (Hoppner & Bittner, 2007). Dependence of PSW activity on the solar flux was also showed in the analysis of long-term wind observations at mesosphere-lower thermosphere heights (Jacobi et al., 2008).

In this study, we use the middle and upper atmosphere model *MUAM* (Pogoreltsev et al., 2007) to perform numerical simulations of the general circulation and PSWs at altitudes from the Earth's surface up to about 300 km. Recently this model was used to investigate the influence of SA on the propagation of stationary planetary waves in the upper atmosphere (Koval et al., 2018). It was shown, that under high SA, the zonal wind speed increases at altitudes above 150 km and decreases in the lower layers. At high SA, the amplitudes of stationary planetary waves decrease above 120 km.

In the current study, we continue this analysis and consider impacts of thermospheric SA changes on the propagation conditions of the westward traveling PSWs with periods 4–16 days generated in the troposphere. Such PSWs correspond to the normal atmospheric modes considered in the theory of atmospheric planetary waves (Longuet-Higgins, 1968). We did not find information about similar previous simulations for a wide set of westward traveling PSW modes. The SA changes were specified in the MUAM model only at the altitudes higher than 100 km (see section 2). Below 100 km, identical conditions corresponding to the medium level of SA were specified. This method allows us to single out the thermospheric influence on the dynamical processes in the atmosphere.

2. The Numerical Model and Solar Activity Accounting

For PSW numerical experiments, the model MUAM (Pogoreltsev, 2007; Pogoreltsev et al., 2007) was used. The model is a modification of the Cologne Model of the Middle Atmosphere-Leipzig Institute for Meteorology (COMMA-LIM; Fröhlich et al., 2003). The MUAM solves the standard set of hydrostatic equations in spherical coordinates described by Gavrilov et al. (2005). Simulations are made for the altitude range from 0 to 300 km, but the weather changes in the troposphere are not modeled. The main simulated parameters include zonal, meridional and vertical velocity components, geopotential, and temperature. The Machuk-Strang splitting procedure (Strang, 1968) is applied, and the scheme proposed by Matsuno (1966) is used for the time integration. To provide the solution stability, a Fourier filter is applied, which limit the zonal resolution to approximately 5°. In the current version of the MUAM, the horizontal grid steps are $5 \times 5.625°$ along the latitude and longitude, respectively. The vertical grid is the log-pressure coordinate $z = H^*\ln(p_0/p)$, where p_0 is the surface pressure and H is the average density scale height. The grid has 56 nodes covering the altitudes from the Earth's surface to about 300 km. The integration time step is 225 s.

The lower boundary conditions are specified at the isobaric level of 1,000 mb in the form of zonal mean climatological distributions of geopotential height and temperature, which are obtained from the JRA-55 (Japanese 55-year Reanalysis) database (Kobayashi et al., 2015) for January by averaging over the years 2005–2014. The MUAM equation for temperature contains an additional term, which is proportional to the

difference between simulated and climatological zonal mean temperature in the tropostratosphere. The proportionality constant corresponds to about 5-day relaxation of the simulated temperature to the climatological one. This allows obtaining more realistic locations and strengths of jet streams in the troposphere. The MUAM involves three-dimensional distributions of ozone in the middle atmosphere, which include averaged over years 1996–2005 climatological inhomogeneities (Suvorova & Pogoreltsev, 2011).

The MUAM involves dynamical and thermal effects of gravity waves (GWs), which are required for the proper simulations of the middle and upper atmosphere (Andrews et al., 1987). These GWs have scales smaller than the MUAM grid spacing and require parameterization. The MUAM uses three such parameterizations. For GWs having small phase speeds (5–30 m/s) a parameterization similar to the Lindzen's one (Lindzen, 1981) is used. For faster waves with phase speeds of 30–125 m/s, which are important in the thermosphere, a version of the spectral parameterization (Yigit & Medvedev, 2009) is applied. The parameterization uses 15 GW spectral components uniformly distributed within the period range from 40 min to 3 hr. The MUAM also involves the parameterization of stationary mountain waves developed and described by Gavrilov and Koval (2013).

Specifying climatological temperature and wind near the lower boundary (see above) generates stationary planetary waves in the MUAM, which were considered by Koval et al. (2018). Besides these waves, the model can simulate traveling modes (Pogoreltsev et al., 2014). Because the MUAM does not adequately replicate the weather in the troposphere, the sources of westward propagating atmospheric normal modes (NMs) in the troposphere were parameterized by inclusion of additional terms to the MUAM equation of heat balance, which involve sets of sinusoidal components versus time with periods corresponding NMs having zonal wave numbers $s = 1$ and $s = 2$. Latitude structures of these terms correspond to the Hough functions of respective NMs calculated with the algorithm by Swarztrauber and Kasahara (1985). NM periods analyzed in this study are equal to the resonant periods of reactions of the atmosphere on the wave forcing at low altitudes, which were determined using a linear model of planetary waves by Pogoreltsev (1999). The present MUAM version takes into account the NMs marked as (1,1), (1,2), (1,3), (2,1), and (2,2) in the classification putted forward by Longuet-Higgins (1968), which, respectively, have periods of 120, 220, 360, 90, and 170 hrs. In this sensitivity consideration, we applied the amplitudes of NM heat sources at altitude of 10 km. These heating sources give simulated NM amplitudes comparable with the observed ones in the stratosphere (Pogoreltsev et al., 2009).

As the original COMMA-LIM (Fröhlich et al., 2003), MUAM contains radiation schemes calculating solar heating and infrared cooling rates of the most prominent absorbers and emitters in the middle atmosphere, such as NO, O, O_2, O_3, H_2O, and CO_2. The model involves parameterizations of radiation heating the atmosphere in the ultraviolet and visible spectral band from 125 to 700 nm and cooling in the 8, 9.6.14, and 15 mkm infrared bands accounting local thermodynamic equilibrium (LTE) disturbances at high altitudes. Also, model includes thermal dissipation from turbulent mixing, ion drag, and molecular heat conduction. Additionally to the radiative scheme used in the original COMMA-LIM version, extreme ultraviolet heating parameterization is included in the thermosphere. Solar fluxes and absorption coefficients for each extreme ultraviolet spectral interval and each constituent were calculated using the model proposed by Richards et al. (1994).

The $F_{10.7}$ flux changes during the 11-year solar activity cycle (e.g., Tapping, 1987). Low and high levels of SA are specified in the MUAM as it was described by Koval et al. (2018). The MUAM radiative block takes into account the dependence of solar radiation on the solar radio flux $F_{10.7}$ at the wavelength of 10.7 cm. The $F_{10.7}$ flux, corresponding to minimum, medium, and maximum SA according to the analysis of the observation data during the last six solar cycles (Royal Observatory of Belgium (ROB), 2013), was set as 70, 130, and 220 sfu (1 sfu = 10^{-22} W/(m^2 Hz)), respectively. As far as we focused only on the thermospheric influence on the global circulation, different $F_{10.7}$ values were set in the MUAM at altitudes above 100 km. Below 100 km, the constant value of $F_{10.7} = 130$ sfu, corresponding to the medium SA level, was set. This approach was applied to isolate the thermospheric influence on the dynamical processes in the atmosphere.

The initial condition for numerical simulations is a windless state with the temperature and geopotential distributions corresponding to the JRA-55 reanalysis database (Kobayashi et al., 2015). For the MUAM adjustment, geopotential heights at the lower boundary are set to be constant in the first 30 model days. Then, the observed geopotential variations corresponding to the JRA-55 database are specified. Before the model day of 121, the MUAM involves the daily mean heating rates only. The tests described by Pogoreltsev (2007) showed that described procedures are enough for the model to reach a steady state

regime at the end of this time interval. After the 121st day, daily variations of heating, parameterization of the NMs, and an additional prognostic equation for the geopotential at the lower boundary are included. This prognostic equation needs to satisfy the lower boundary condition for the waves generated by internal sources (Pogoreltsev et al., 2007, 2009). Starting from the 330th model day, seasonal changes in solar heating are triggered and the next 60 days are considered as characteristic for January–February.

The results of a MUAM run may depend on particular phases of simulated NMs. In addition, relatively small variations in the initial conditions can have a substantial influence on the evolution of the simulated fields (e.g., Gray et al., 2003; Yoden, 1990). Both NM phases and initial perturbations can be accounted by changing the day of inclusion of atmospheric NMs and prognostic equation for geopotential height at the lower boundary mentioned above during the initial MUAM adjustment. In the present study, we simulated ensembles of 12 MUAM runs with the day of NM source activating varying between 120 and 131 with the step of 1 day.

To include the influence of charged particles in the ionosphere on the neutral gas dynamics, conductivities of the ionosphere and their longitudinal, latitudinal, and temporal dependences were calculated (Dickinson et al., 1975; Shevchuk et al., 2018). Zonal and meridional coefficients of the ion drag I_λ, I_φ, and geomagnetic torque M are calculated using the formulae

$$I_\lambda = -\frac{\sigma_1 H_0^2}{\rho c^2}, I_\varphi = -\frac{\sigma_1 H_z^2}{\rho c^2}, \quad M = \frac{\sigma_2 H_z H_0}{\rho c^2}, \tag{1}$$

where H_z and H_0 are the vertical component and module of the vector of magnetic field intensity, respectively; ρ is the density of the neutral atmosphere; c is the light speed; σ_2 and σ_1 are the Hall and Pedersen ionospheric conductivities, respectively. They are calculated using formulae (e.g., Pogoreltsev, 1996)

$$\sigma_1 = eN\left(\mu_1^e + \mu_1^i\right); \quad \sigma_2 = eN\left(\mu_2^e - \mu_2^i\right), \tag{2}$$

where N and e are the number electron density and the electron charge, respectively, $\mu_1^i, \mu_2^i, \mu_1^e, \mu_2^e$ are, respectively, the prea-mobility of ions and electrons.

Parameters of the ionosphere and thermosphere are taken from the semiempirical models of the ionosphere IRI-Plas (Gulyaeva et al., 2002) and atmosphere NRLMSISE-00 (Picone et al., 2002). The ion drag and geomagnetic torque (1) with their diurnal variations for January were included into the MUAM at 23 altitude grid nodes above 100 km at all longitudes and latitudes.

In order to analyze the results of numerical simulations of PSW amplitudes, the latitude-altitude distributions of the mean zonal quasi-geostrophic complex refractivity index squared (RI^2) were calculated by the formulae (1) in Gavrilov et al. (2015). According to Dickinson (1968) and Matsuno (1970), PSWs should propagate in regions of the atmosphere where RI^2 is positive and becomes evanescent at negative RI^2 values, so areas of the positive RI^2 are considered as the waveguides. The boundaries of these waveguides are located frequently near PSW critical levels, where zonal wind is approximately equal to PSW horizontal phase speed.

Considering changes in RI^2, one can study the relative importance of the strength, shear, and curvature of the zonal mean wind influencing the trajectories of PSW propagation. For further diagnostics of the PSW propagation, the Eliassen-Palm flux (EP-flux) vector was calculated by the formulae (2) in Gavrilov et al. (2015). An upward direction of EP-flux vector relates to the northward wave heat flux, while southward EP-flux vector relates to the northward PSW momentum flux. The divergence of the EP-flux shows the net drag of the zonal mean flow by the PSWs. In case of steady, low-frequency waves, their group velocity is parallel to the EP-flux vector. Besides this, the EP-flux vector is curved up the gradient of RI^2 and particularly, is directed along the regions of positive RI^2 (Karoly and Hoskins, 1982). Thus, RI^2 and EP-flux vector could be useful tools for analyzing and visualizing the PSW propagation trajectories in the latitude-altitude plane.

3. Results of Simulation

In order to distinguish changes in the thermosphere due to SA and their effects on PSW amplitudes, two 12-member ensembles of model runs with conditions corresponding to the high and low SA (see section 2) were calculated. Different levels of SA were specified in the MUAM at altitudes above

100 km similar to the study by Koval et al. (2018). Below this altitude, medium SA level was set in the MUAM for all model runs. Wind, temperature, and geopotential fields were simulated for January–February. The longitude-time Fourier transform of the MUAM solutions with the least squares fitting of the hydrodynamic fields (geopotential height, wind, and temperature) estimated the PSW amplitudes and phases.

We analyzed the average over 12 model runs differences in amplitudes of PSWs corresponding to atmospheric NMs with zonal wave numbers s = 1–2 and periods of 4–16 days, caused by SA changes in the thermosphere. Averaging over 12 model runs and over 2 months allows us to improve statistical confidence and diminish effects of the sudden stratospheric warming events, which could occur at different times in individual MUAM runs.

3.1. PSW Amplitudes and Phases

Latitude-altitude dependences of the zonal mean wind, temperature, and meridional gradient of temperature are averaged over 12 MUAM runs and over January–February; also, their differences between high and low SA are presented in the supporting information Figures S1–S3. Simulated temperature generally match to semiempirical model of temperature NRLMSISE-00 (Picone et al., 2002) for different SA levels as shown in Figure S4 in the supporting information. Zonal circulation is consistent with semiempirical horizontal wind model HWM07 (Drob et al., 2008). At heights above 160–180 km, the zonal wind is smaller at low SA in both hemispheres. Between 180 and 140 km the zonal velocity is larger at high SA in the Southern Hemisphere. This is associated with corresponding differences of the meridional temperature gradient in the right panel of supporting information Figure S4.

At heights below 100 km in Figure S1, Koval et al. (2018) found minor differences in zonal velocity between high and low SA. For instance, the differences in the zonal mean velocity may become 3 m/s (about 6%) in the midlatitude Northern Hemisphere at heights 60–100 km. Estimations of statistical significance with paired Student's t test (e.g., Rice, 2006) using $12 \times 720 \times 64 = 552{,}960$ pairs of respective values for the low and high SA (obtained from 12 model runs, 720 two-hour outputs at 64 longitude grid nodes) gave 99% statistical significance of the mentioned above mean zonal wind differences at heights below 100 km (Koval et al., 2018). This gives evidences that changes in thermospheric parameters produced by SA variations at heights above 100 km may affect the global circulation at altitudes of the middle atmosphere.

Figure 1 reveals simulated latitude-height distributions of PSW amplitudes averaged over January–February for two 12-member ensembles of model runs under high and low SA; also, their differences due to SA changes in the thermosphere. Here and in the next figures, the globally averaged geopotential height has been used as vertical coordinate. In Figure 1 one can see that the main maxima of 7-, 10-, and 16-day PSWs exist at the middle and high latitudes of the Northern (winter) Hemisphere. Amplitudes of 4 and 5 days have maxima also in the Southern (summer) Hemisphere, which are stronger at low SA at heights above 100 km, especially for the 5-day PSW (see the middle panel of Figure 1b). This can be connected with the largest westward phase speed of the traveling 5-day NM in the middle atmosphere (e.g., Gavrilov et al., 2015).

Differences in PSW amplitudes between high and low levels of SA are shown in the right panels of Figure 1. The paired Student's t test (Rice, 2006) was applied to the ensembles of 12 pairs of simulated PSW amplitudes for the high and low SA levels at each latitude and altitude location. The areas where t test gave smaller than 95% statistical confidence of nonzero amplitude differences are shaded with lines in the right panels of Figure 1. One can see that statistically significant differences can exist at heights above 100–150 km.

Respective differences in the zonal mean velocity and temperature fields caused by changes from high to low SA can be found in the supporting information Figures S1 and S2. Changes in general circulation can modify spatial distributions of PSW amplitudes. Under the high SA, PSW amplitudes are generally (up to 100%) smaller at thermospheric heights. The most significant decrease at high SA for the 16-day PSW amplitude can be seen in the right panel of Figure 1e at heights above 200 km. The eastward direction of atmospheric circulation during the winter season in the Northern Hemisphere contributes to better propagation of planetary waves (e.g., Charney & Drazin, 1961). In the middle and high latitudes of the Southern Hemisphere, largest negative differences one can see in the right panel of Figure 1b at altitudes above 150 km.

Magnitudes and structure of simulated 5-day PSWs are in general agreement with those obtained from TIMED/SABER temperature measurements at altitudes of the middle atmosphere, mesosphere and lower

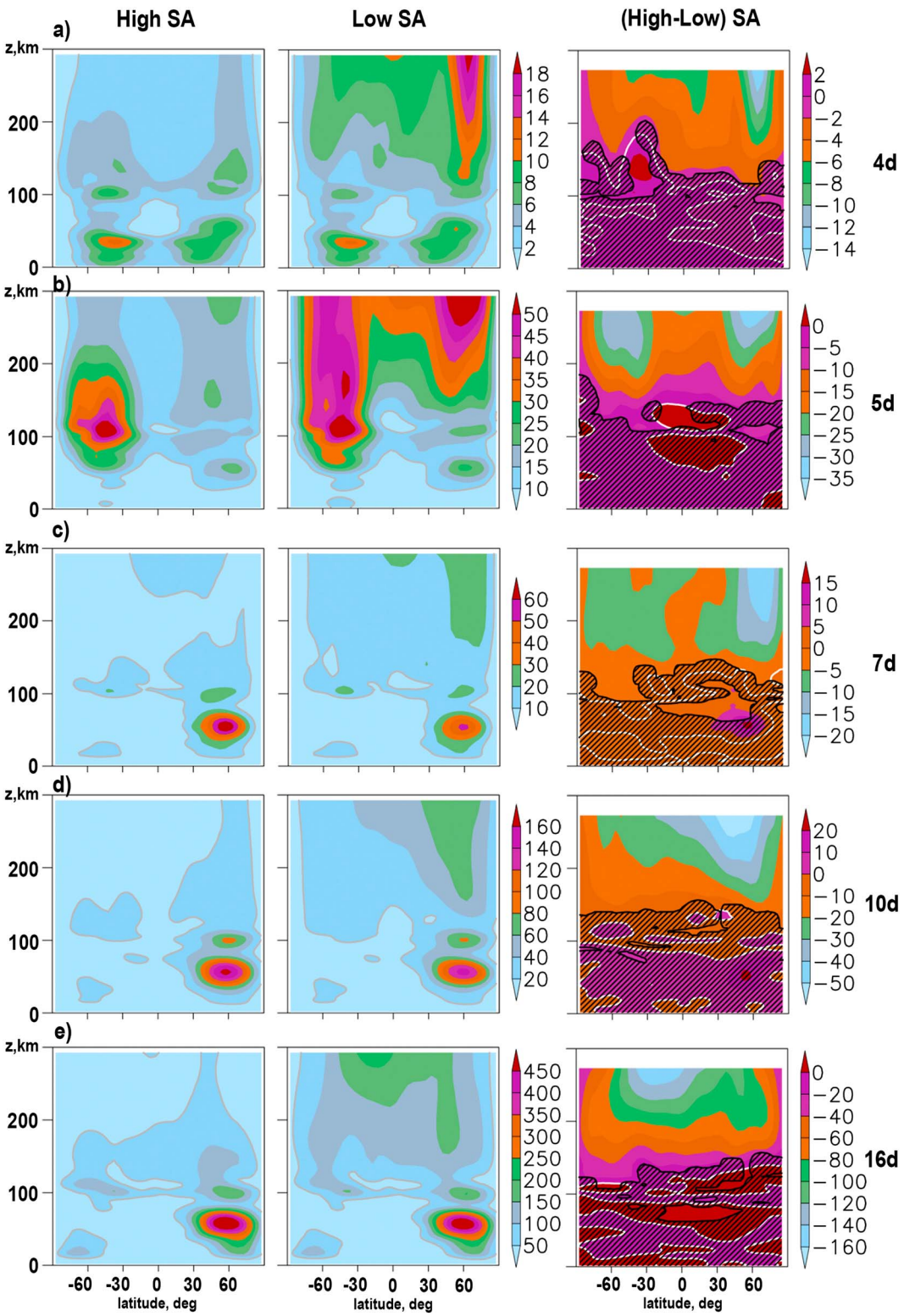

Figure 1. Amplitudes of the geopotential height variations (in g.P.m.) caused by the westward traveling PSWs with periods 4, 5, 7, 10, and 16 days (a–e, respectively) under the high SA (left), low SA (middle), and their differences (right) averaged over 12-member ensembles and over January–February. Areas shaded with lines show regions with statistical confidence of respective differences smaller than of 95% according to paired Student's *t* test.

thermosphere (Pancheva et al., 2010; Riggin et al., 2006). Simulated 10-day PSW corresponds to the Broadband Emission Radiometry temperature measurements at altitudes below 100 km and latitudes between −50°S and 50°N averaged over the years 2002–2013 (Forbes & Zhang, 2015). The existence of the simulated PSW modes with the same periods in the ionosphere was confirmed by many observations of the total electron content at different latitudes (e.g., Borries et al., 2007; Pedatella & Forbes, 2009).

At altitudes below 100 km, the right panels of Figure 1 demonstrate mainly positive differences corresponding to larger PSW amplitudes under high SA. In the considered model, a possible mechanism of amplitude variations in the middle atmosphere could be partial reflection of upward propagating PSWs at heights of the lower thermosphere due to substantial increase in the thermospheric temperature at high SA (see Figure S2 in THE supporting information). Similar effects were also found in previous studies (e.g., Lu et al., 2017). Stronger reflection could cause PSW amplitude decreases under the high SA in the thermosphere (see above). However, the statistical confidence of the right panels of Figure 1 is not adequate at altitudes below 100 km. Further studies with larger number of model runs are required for better statistical confidence of PSW amplitude changes in the middle atmosphere caused by SA variations.

Phases of the PSWs were also analyzed. Strong phase shifts exist at altitudes of 80–100 km for 5-, 10-, and 16-day PSWs having the zonal wave number 1, especially at low SA. This could be connected with possible influence of plasma drift on PSW propagation into the lower ionosphere and on the wave phases (Laštovicka, 2006). Temporal time lag in PSWs propagating into the lower ionosphere up to several days were found by Pancheva et al. (1994) and by Stray and Espy (2018).

3.2. PSW Refractivity Index and Eliassen-Palm Flux

The RI^2 and EP-flux vectors corresponding to Figure 1 are shown in Figure 2. Theory of planetary waves predicts waveguides in the regions of positive RI^2 (see section 2). Values of RI^2 depend on the zonal mean wind and temperature (Andrews et al., 1987). The left and middle panels of Figure 2 show that regions of positive RI^2 for westward traveling PSWs exist in both Northern and Southern Hemispheres. At altitudes above 120 km the regions of positive RI^2 are wider and more homogeneous than those at lower altitudes. Comparisons of the left and middle panels of Figure 2 reveal differences in RI^2 values in the thermosphere, which can influence PSW propagation.

Vectors of EP-fluxes in the left and middle panels of Figure 2 correspond to the westward traveling PSWs generated mainly in the middle atmosphere. Then their energy can propagate upward along the waveguides. Above, Figure 1 showed that the 4- and 5-day PSWs have substantial amplitudes in the thermosphere of the Southern Hemisphere, while amplitudes of longer-period PSWs having slower horizontal phase speeds are relatively small there. The left and middle panels of Figure 2 reveal regions of negative RI^2 in the Southern Hemisphere at altitudes below 100 km. The regions of negative RI^2 in the left and middle panels of Figures 2c–2e for longer-period PSWs are larger than those for the 4- and 5-day PSWs in Figures 2a and 2b. Therefore, longer-period PSWs may have worse conditions for their propagation in the middle atmosphere of the Southern Hemisphere, which can explain smaller amplitudes of longer-period PSWs in the southern thermosphere in Figure 1.

The main maxima of 5-day PSW at altitudes 100–150 km in the Southern Hemisphere in Figure 1b can be attributed to longer EP-flux vectors in these regions in Figure 2b. Similarly, longer EP-flux vectors exist at altitudes 50–70 km in the midlatitude Northern Hemisphere in Figures 2c–2e, where the main maxima of the 7-, 10-, and 16-day PSWs are located in Figures 1c–1e.

Contrary to the 4- and 5-day PSWs, longer-period wave modes have larger amplitudes in the middle atmosphere than those in the thermosphere in Figures 1c–1e. This may be connected with amplification of the PSW amplitudes in the middle atmosphere caused by partial reflection of upward propagating waves from the lower thermosphere (Lu et al., 2017). Considerations of the left and middle panels of Figure 2 reveal regions of increased RI^2 at altitudes 100–130 km at middle and high latitudes of the Northern Hemisphere. Increased vertical gradients of RI^2 in these regions may produce increasing partial reflection of PSWs propagating from the lower atmospheric layers. Figure 2 shows that mentioned regions of $RI^2 > 0$ at altitudes 100–130 km are larger and can span up to the North Pole for the 7-, 10-, and 16-day PSWs. This can confirm a possibility of larger reflection of longer-period PSWs in the regions of lower thermosphere.

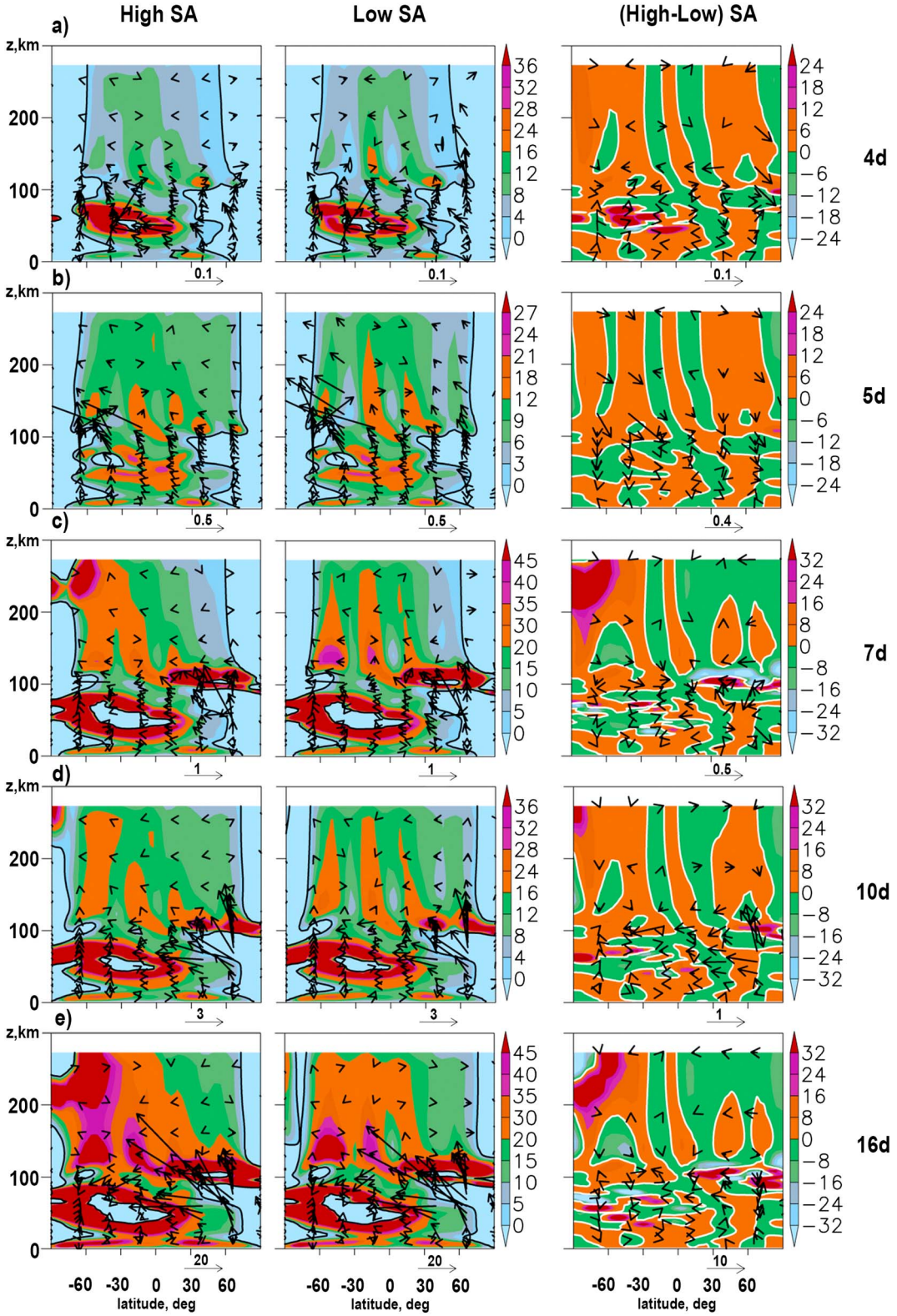

Figure 2. Normalized refractivity index squared (colors) and corresponding EP-flux (m^3/s^2; arrows) produced by the westward traveling PSWs with periods 4, 5, 7, 10, and 16 days (a–e, respectively) under the high SA (left), low SA (middle), and their differences (right). Solid contours in panels correspond to zero values.

At middle and high latitudes of the Southern Hemisphere in the left and middle panels of Figure 2, one can see layers of increased RI^2 for the 7-, 10-, and 16-day PSWs at altitudes below 100 km and above 200 km. Possible partial reflections from these layers may explain small amplitudes of longer-period PSWs at altitudes above 200 km in the southern thermosphere (see Figure 1).

In some cases, EP-flux vectors in Figure 3 are originating in the regions, where $RI^2 < 0$ and PSW propagation from below is not allowed. This may assume possible PSW generation in the middle and upper atmosphere.

The right panels of Figure 2 show differences in RI^2 and EP-flux vectors between high and low SA levels. In the Northern Hemisphere, maximum positive and negative RI^2 differences exist at altitudes 90–120 km at middle and high latitudes for the 7-, 10-, and 16-day PSWs. These differences may cause changes in PSW partial reflection and in the proportion of wave energy propagating to the thermosphere. According to Figure 1, such partial reflection should be stronger at high SA, which corresponds to smaller amplitudes of longer-period PSWs at altitudes above 100 km. In the Southern Hemisphere, maximum RI^2 differences for longer-period PSWs occur at middle and high latitudes at altitudes below 100 km and above 200 km. Increased partial reflections of longer-period PSWs in these regions may cause smaller wave amplitudes in the southern thermosphere at high SA in Figure 1.

The differences in EP-flux vectors in the right panels of Figures 2c–2e for longer-period PSWs are directed frequently toward the equator at altitudes below 100 km in the Northern Hemisphere, which corresponds to larger southward EP-fluxes at high SA. This is most noticeable in the right panel of Figure 2d for the 10-day PSW. It may be connected with larger partial reflection of longer-period PSWs propagating to the thermosphere at high SA (see above) and with respective redistributions of vertical and horizontal EP-fluxes.

In many cases, vector differences in EP-flux have components directed upward and downward at high latitudes in the right panels of Figure 3. This could be additional reasons for changes in general circulation at different altitudes. According to theory, the upward and downward vertical components of EP-flux correspond to northward and southward directions of the PSW heat flux (e.g., Andrews et al., 1987). Therefore, vertical directions of EP-flux differences in Figure 3 may correspond to the warmer or cooler North and South Poles, which can influence general circulation of the atmosphere (Holton & Mass, 1976).

3.3. Other Hydrodynamic Fields

In section 3.1, the analysis of PSW amplitudes was made for geopotential height simulated with the MUAM. For comparisons with experiments, information about PSW amplitudes for the other hydrodynamic fields is valuable. Figures 3–5 are similar to Figure 1 and represent amplitudes of westward traveling PSWs for eastward, u, northward, v, wind components, and temperature, T, respectively.

Westward traveling PSWs were observed at different altitudes in the stratosphere, mesosphere, and thermosphere with different methods. Mitchell et al. (1999) used radio meteor radar and analyzed amplitudes of PSW wind variations with periods around 16 days at altitudes 80–100 km and latitude of 54°N. They found amplitudes up to 14 m/s in January, which is comparable with the 16-day PSW amplitudes in Figures 3e and 4e. Day et al. (2012) studied amplitudes of the 16-day and 5-day PSWs in the mesosphere and lower thermosphere using radio meteor wind measurements and temperature data from the Aura satellite. At altitudes 80–100 km and latitude of 42° they found amplitudes of several meters per second for wind and several kelvin for temperature for the 16-day and 5-day PSWs, which satisfactorily match to Figures 3b, 3e, 5b, and 5e.

The analysis of 16-day PSW at altitudes 10–90 km was performed by Day et al. (2011) from the observations with the Microwave Limb Sounder on the Aura satellite in years 2004–2010. They showed maxima of temperature wave variations up to 8 K at latitudes 40–75°N and altitudes 30–50 km and 60–80 km in January–February and amplitudes smaller than 1–2 K in the middle atmosphere of the Southern Hemisphere. This corresponds to the PSW amplitude structure at altitudes below 100 km, in the left and middle panels of Figure 5.

Garcia et al. (2004) analyzed the 5-day PSW in the mesosphere and lower thermosphere observed with the SABER instrument on the TIMED satellite in years 2001–2004. They found large temperature amplitudes of the 5-day PSW up to 2.5–3.5 K both in the Northern and Southern Hemispheres. The amplitudes are comparable with those shown in Figure 5b and confirm propagation of westward 5-day PSW in both hemispheres.

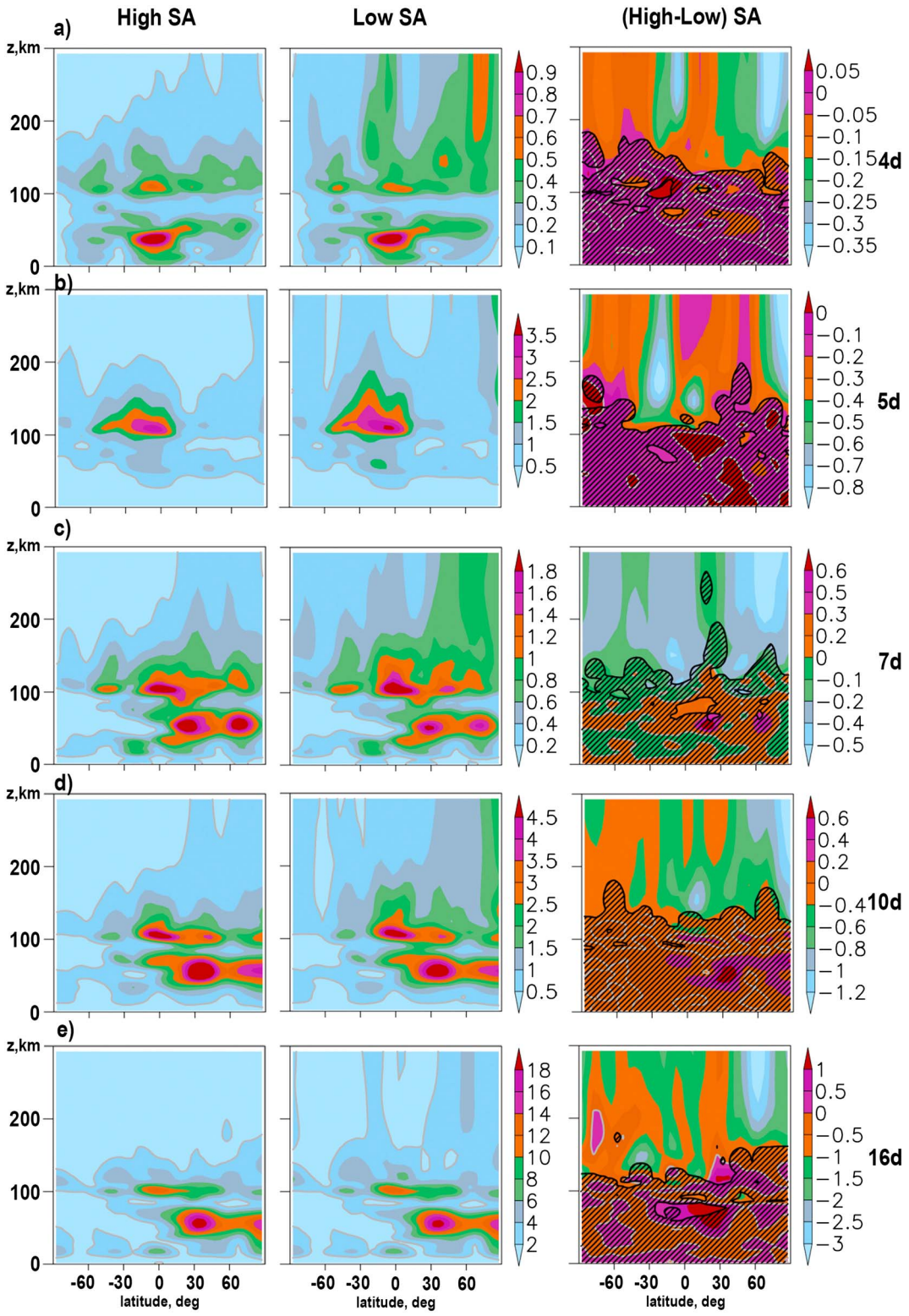

Figure 3. Same as Figure 1 but for zonal velocity in meters per second.

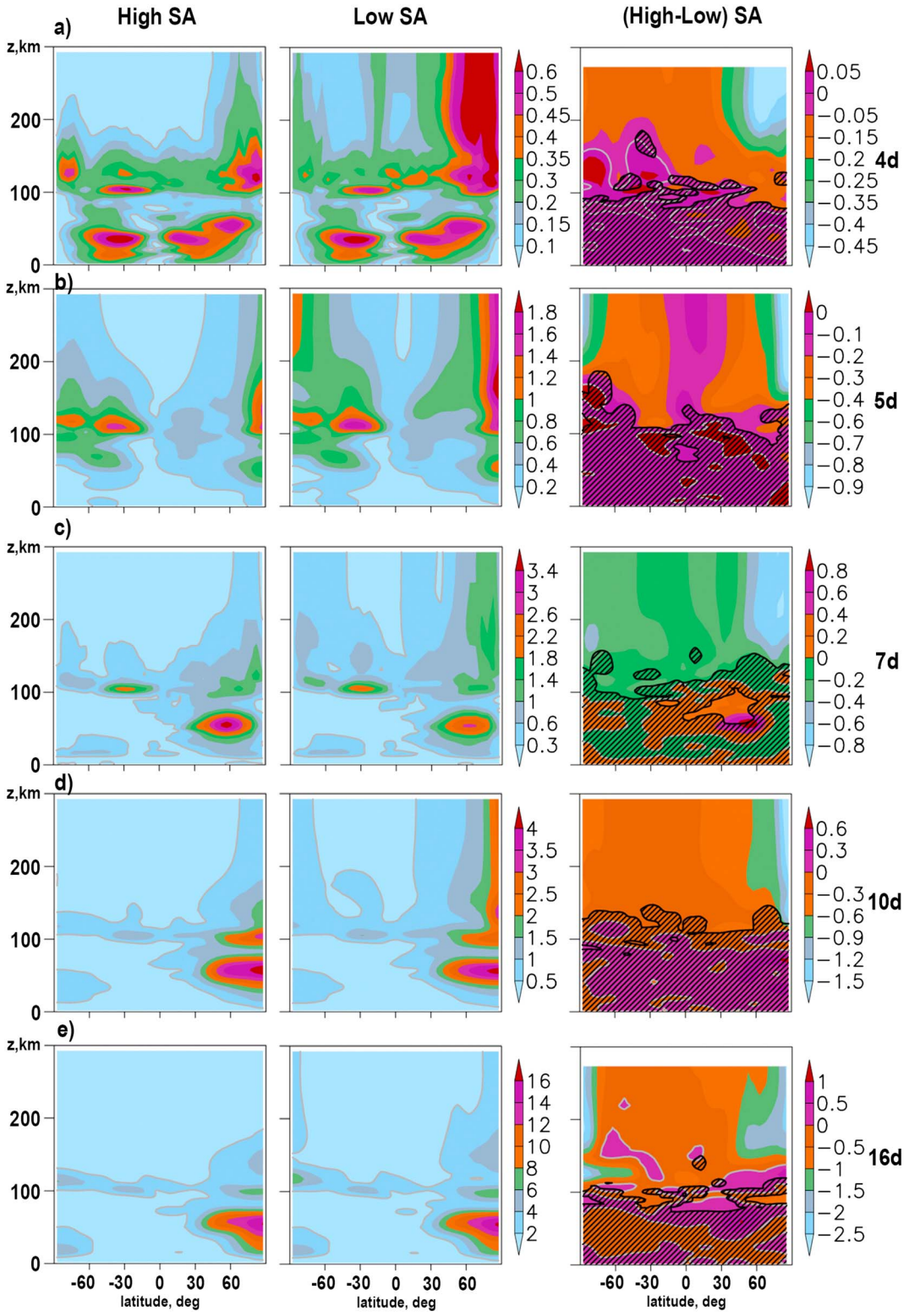

Figure 4. Same as Figure 1 but for meridional velocity in meters per second.

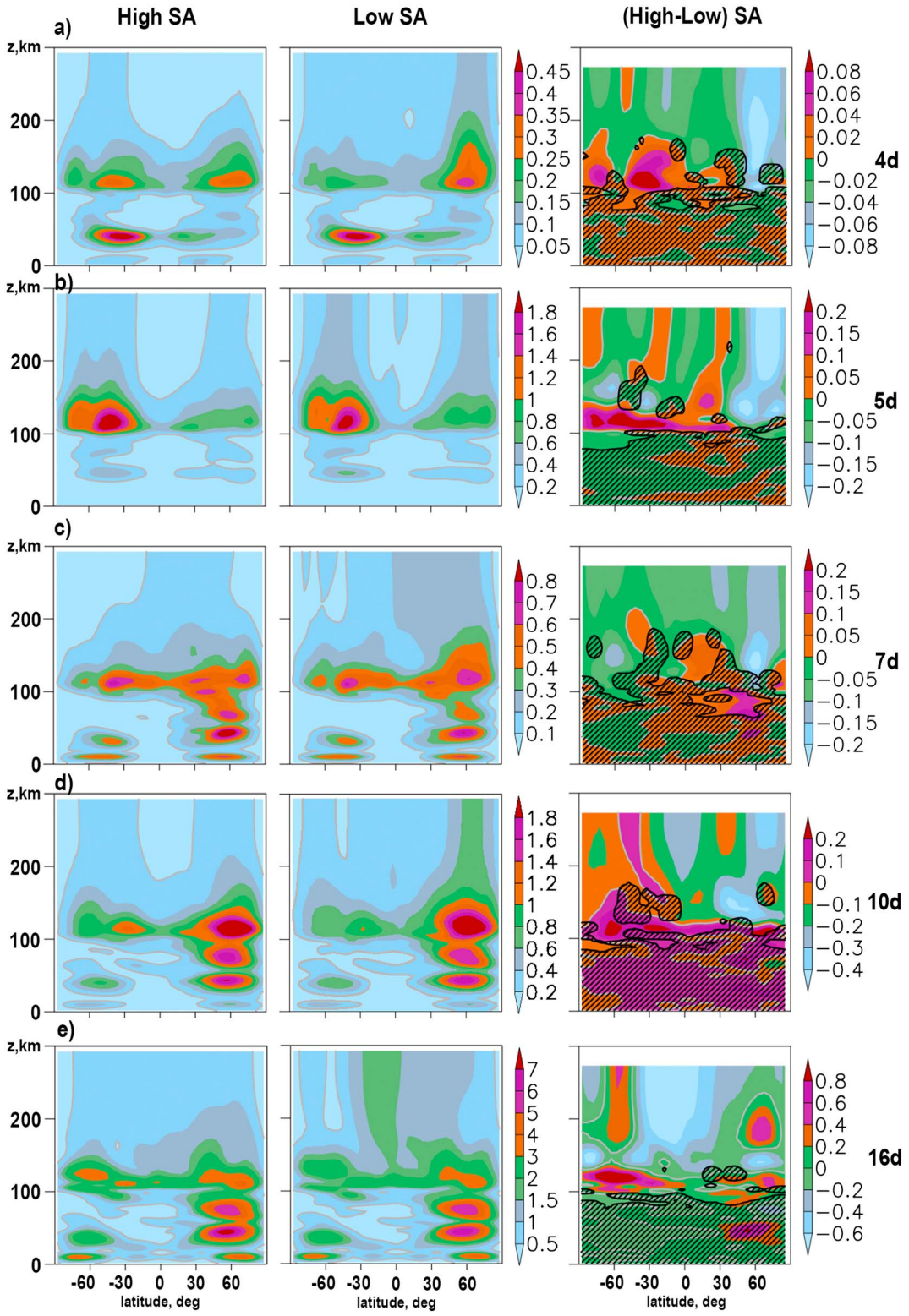

Figure 5. Same as Figure 1 but for temperature in kelvin.

4. Discussion

Comparisons of PSW amplitudes of Figures 3–5 in the troposphere and lower stratosphere with analyses of respective PSW modes from the meteorological reanalysis data bases (e.g., JRA-55, Kobayashi et al., 2015) show that the amplitudes of tropospheric PSW sources in the present simulations correspond to climatological level of PSW activity. Observations of PSWs in the thermosphere sometimes show larger values of their amplitudes than shown in Figures 1 and 3–5 (e.g., Borries & Hoffmann, 2010; Gu et al., 2014). Such intensive PSWs may correspond to existence of local intensive wave sources. Many experiments described in the literature were performed in other seasons than considered here northern winter. In addition, such intensive PSWs are supposed to be amplified in the thermosphere by nonlinear wave-wave and wave-mean flow interactions involving tides (e.g., Forbes et al., 2018; Laštovicka, 2006; Yamazaki & Richmond, 2013) and plasma drifts (Liu & Richmond, 2013). The main goals of the present study are relative changes in PSW characteristics at different SA levels, which are less sensitive to absolute wave amplitudes.

One may have concern that PSW amplitudes in the thermosphere shown in Figures 1, and 3–5 could not reflect PSWs propagating from the lower atmosphere, but can be produced by the mathematical noise and nonlinear interactions in the MUAM during simulations. Control MUAM runs with zero tropospheric NM sources showed that MUAM indeed can generate westward traveling PSWs (see supporting information Figures S5 and S6); however, in the thermosphere they are noticeable mainly at low SA at high latitudes of the Northern Hemisphere, where their amplitudes are 2–4 times smaller than those presented in Figure 1. Therefore, for considered waves, these figures represent mainly amplitudes of PSWs propagating to the thermosphere from NM sources located near the lower boundary of the MUAM.

Considerations of Figures 1 and 3–5 show that westward traveling PSWs propagating from the lower atmosphere in January–February can have generally higher amplitudes in the thermosphere at high latitudes of the Northern Hemisphere. Amplitudes of PSW variations of u, v, and T in Figures 3–5 decreases above altitude of 100 km, but they are still noticeable at altitudes up to 200 km and above, especially under low solar activity conditions. At high altitudes, variations of geopotential height could be more sensitive to PSWs, propagating from the lower atmosphere, because their amplitudes increase in altitude for many PSW modes in Figure 1.

Figure 1 and, especially, Figures 3–5 show sharp increases in PSW amplitudes just above altitude of 100 km. This could be connected with sharp increases in Brunt-Vaisala frequency N due to big vertical temperature gradients in the lower thermosphere. The wave activity flux, $\boldsymbol{F_a}$, can be represented in the form of $\boldsymbol{F}_a = \boldsymbol{c}_g A$, where $\boldsymbol{c}_g$ is the group speed and A is the wave activity (Andrews et al., 1987). The vertical component of group velocity $c_{gz} \sim m^{-1}$, where m is the vertical wave number. According to the PW dispersion equation (e.g., Andrews et al., 1987), an increase in N leads to increasing m. Discontinuity of the vertical component of the wave activity flux F_{az} at increasing m requires respective increase in the wave activity A and in PSW amplitudes. The main regions of positive vertical gradients of temperature and expected increasing A are the stratosphere and the lower thermosphere. Figures 1 and 3–5 reveal maxima of PSW amplitudes in these regions. Vertical temperature gradients in the lower thermosphere are larger during high solar activity. Therefore, one should expect larger increase in PSW amplitudes at high SA. Indeed, PSW amplitudes in Figures 3–5 at altitudes 100–120 km are in many cases larger at high SA compared to low SA, especially for temperature.

Increased PSW amplitudes and vertical wave numbers (corresponding to shorter vertical wavelengths) produce larger vertical gradients of all hydrodynamic fields in the lower thermosphere, which are subjects for stronger molecular and turbulent dissipation at high SA compared to low SA. Additionally, higher ion content produce stronger ion viscosity increasing PSW dissipation during high SA. This may explain generally smaller amplitudes of westward traveling PSWs in the thermosphere at high SA found in Figures 1 and 3–5.

Increased vertical temperature gradients and Brunt-Vaisala frequency in the lower thermosphere can also lead to partial reflections of PSWs propagating from below (Arnold & Robinson, 1998; Geller & Alpert, 1980). Temperature gradients and partial reflection should be stronger at high SA, which can contribute to a smaller proportion of PSW energy penetrating to the thermosphere and to smaller PSW amplitudes in the thermosphere at high SA in Figures 1 and 3–5.

Partial PSW reflection in the lower thermosphere and differences in RI^2 and EP-flux vectors at altitudes below 100 km shown in the right panels of Figure 2 may cause differences in PSW characteristics and the zonal mean circulation in the middle atmosphere at different SA levels. The right panels of Figures 1 and 3–5

demonstrate some differences in the amplitudes of westward propagating PSWs at altitudes below 100 km. However, it was discussed above that the statistical significance of these differences is not adequate at altitudes below 100 km. Therefore, further simulations with larger number of model runs are required for more statistically reliable conclusions about the role of changes in partial reflection of PSWs from the thermosphere in possible influence of SA on the dynamics of the middle atmosphere.

5. Conclusion

The amplitudes and phases of westward traveling PSWs with the zonal wave numbers s = 1–2 and periods 4–16 days generated near the ground were calculated for the first time under high and low SA at altitudes from the Earth's surface up to 300 km. The effects of SA changes in the thermosphere on the low-amplitude PSW propagation and reflection conditions were studied. For this purpose, the thermospheric version of the MUAM numerical model was utilized. The two 12-member ensembles of simulations of general circulation for the conditions corresponding to low and high SA were obtained.

To single out influence of the thermosphere, the SA changes were included into the MUAM at heights above 100 km only. The indicator of SA in the MUAM is the solar radio flux at the wavelength of 10.7 cm. The impact of ionospheric charged particles on the neutral gas motion was accounted in the MUAM by including the ionospheric conductivities and their spatial and temporal inhomogeneities for different SA levels. Refractivity indices and EP-fluxes corresponding to the observed PSW modes were calculated.

In the model, the westward traveling PSWs are generated at the lower boundary, then their energy can propagate upward along the waveguides. The 4- and 5-day PSWs have comparable amplitudes of geopotential height variations in both hemispheres, while PSWs with lower horizontal phase speeds have amplitude maximums in the Northern Hemisphere because of spacious regions with $RI^2 < 0$ in the middle atmosphere of the Southern Hemisphere. Regions of maximum PSW amplitudes correlate with the maxima in their EP-fluxes.

The 7-, 10-, and 16-day waves have significantly larger geopotential height amplitudes in the middle atmosphere than in the thermosphere. It can be explained by both the partial reflection and changes in PSW propagation conditions in the lower thermosphere. Changes in the background zonal velocity and temperature caused by the SA variations can modify spatial distributions of the westward traveling PSWs. Wave amplitudes are significantly (up to 100%) smaller at the thermospheric heights under high SA, which is accompanied by a smaller EP-flux vertical component. The most significant decrease in the PSW amplitude in the thermosphere is found for the 16-day wave.

The statistical significance of nonzero differences in PSW amplitudes between the high and low SA conditions is higher than 95% at altitudes above 100–150 km. For more reliable conclusions about the SA influence in the lower and middle atmosphere, more statistically significant numerical modeling is required. In addition, the simulations should involve not only thermospheric influence but also effects of changes in solar irradiance and cosmic rays intensity on the dynamical processes in the middle atmosphere.

Acknowledgments
The authors thank two reviewers for helpful and constructive comments that were used in revising the manuscript. The adjustment and launching of the MUAM model, simulating general circulation were supported by the Council on Grants of the President of the Russian Federation (MK-1424.2017.5). The calculations of the PSW amplitudes, EP-fluxes, and refractivity indices, analyzing the results of simulations were supported by the Russian Foundation for Basic Research (16-35-60013 mol_a_dk). All data sets presented in the paper can be freely accessed at https://doi.org/10.5281/zenodo.1322332. According to the statement 1296 of the Civil Code of the Russian Federation, all rigths on the MUAM code belong to the Russian State Hydrometeorological University (RSHU). To get access to the computer codes and for their usage, a reader should get a permission from the RSHU Rector at the address listed in the beginning of the paper. The authors can assist in getting such permission.

References

Akmaev, R. A. (2011). Whole atmosphere modeling: Connecting terrestrial and space weather. *Reviews of Geophysics*, *49*, RG4004. https://doi.org/10.1029/2011RG000364

Andrews, D. G., Holton, J. R., & Leovy, C. B. (1987). *Middle atmosphere dynamics* (p. 489). New York: Acad. Press.

Arnold, N. F., & Robinson, T. R. (1998). Solar cycle changes to planetary wave propagation and their influence on the middle atmosphere circulation. *Annales Geophysicae*, *16*(1), 69–76. https://doi.org/10.1007/s00585-997-0069-3

Borries, C., & Hoffmann, P. (2010). Characteristics of *F*2-layer planetary wave-type oscillations in northern middle and high latitudes during 2002 to 2008. *Journal of Geophysical Research*, *115*, A00G10. https://doi.org/10.1029/2010JA015456

Borries, C., Jakowski, N., Jacobi, C., Hoffmann, P., & Pogoreltsev, A. I. (2007). Spectral analysis of planetary waves seen in ionospheric total electron content (TEC): First results using GPS differential TEC and stratospheric reanalyses. *Journal of Atmospheric and Solar - Terrestrial Physics*, *69*(17-18), 2442–2451. https://doi.org/10.1016/j.jastp.2007.02.004

Chang, L. C., Liu, J. Y., & Palo, S. E. (2011). Propagating planetary wave coupling in SABER MLT temperatures and GPS TEC during the 2005/2006 austral summer. *Journal of Geophysical Research*, *116*, A10324. https://doi.org/10.1029/2011JA016687

Chang, L. C., Yue, L., Wang, W., Wu, Q., & Meier, R. R. (2014). Quasi two day wave-related variability in the background dynamics and composition of the mesosphere/thermosphere and the ionosphere. *Journal of Geophysical Research: Space Physics*, *119*, 4786–4804. https://doi.org/10.1002/2014JA019936

Chanin, M.-L. (2006). Signature of the 11-year cycle in the upper atmosphere. *Space Science Reviews*, *125*(1-4), 261–272. https://doi.org/10.1007/s11214-006-9062-5

Charney, J. G., & Drazin, P. G. (1961). Propagation of planetary-scale disturbances from the lower into the upper atmosphere. *Journal of Geophysical Research*, *66*(1), 83–109. https://doi.org/10.1029/JZ066i001p00083

Day, K. A., Hibbins, R. E., & Mitchell, N. J. (2011). Aura MLS observations of the westward-propagating 16-day planetary wave in the stratosphere, mesosphere and lower thermosphere. *Atmospheric Chemistry and Physics*, *11*(9), 4149–4161. https://doi.org/10.5194/acp-11-4149-2011

Day, K. A., Taylor, M. J., & Mitchell, N. J. (2012). Mean winds, temperatures and the 16- and 5-day planetary waves in the mesosphere and lower thermosphere over bear Lake observatory (42° N, 111° W). *Atmospheric Chemistry and Physics*, *12*(3), 1571–1585. https://doi.org/10.5194/acp-12-1571-2012

Dickinson, R. E. (1968). Planetary Rossby waves propagating vertically through weak westerly wave guides. *Journal of the Atmospheric Sciences*, *25*(6), 984–1002. https://doi.org/10.1175/1520-0469(1968)025<0984:PRWPVT>2.0.CO;2

Dickinson, R. E., Ridley, E. C., & Roble, R. G. (1975). Meridional circulation in the thermosphere - 1. Equinox conditions. *Journal of the Atmospheric Sciences*, *32*(9), 1737–1754. https://doi.org/10.1175/1520-0469(1975)032<1737:MCITTI>2.0.CO;2

Drob, D. P., Emmert, J. T., Crowley, G., Picone, J. M., Shepherd, G. G., Skinner, W., et al. (2008). An empirical model of the Earth's horizontal wind fields: HWM07. *Journal of Geophysical Research*, *113*, A12304. https://doi.org/10.1029/2008JA013668

Forbes, J. M., & Zhang, X. (2015). Quasi-10-day wave in the atmosphere. *Journal of Geophysical Research: Atmospheres*, *120*, 11,079–11,089. https://doi.org/10.1002/2015JD023327

Forbes, J. M., Zhang, X., Maute, A., & Hagan, M. E. (2018). Zonally symmetric oscillations of the thermosphere at planetary wave periods. *Journal of Geophysical Research: Space Physics*, *123*, 4110–4128. https://doi.org/10.1002/2018JA025258

Forbes, J. M., Zhang, X., Ward, W., & Talaat, E. R. (2002). Climatological features of mesosphere and lower thermosphere stationary planetary waves within ±40 latitude. *Journal of Geophysical Research*, *107*(D17), 4322. https://doi.org/10.1029/2001JD001232

Fröhlich, K., Pogoreltsev, A., & Jacobi, C. (2003). Numerical simulation of tides, Rossby and kelvin waves with the COMMA-LIM model. *Advances in Space Research*, *32*(5), 863–868. https://doi.org/10.1016/S0273-1177(03)00416-2

Gan, Q., Du, J., Fomichev, V. I., Ward, W. E., Beagley, S. R., Zhang, S., & Yue, J. (2017). Temperature responses to the 11 year solar cycle in the mesosphere from the 31year (1979–2010) extended Canadian middle atmosphere model simulations and a comparison with the 14year (2002–2015) TIMED/SABER observations. *Journal of Geophysical Research: Space Physics*, *122*, 4801–4818. https://doi.org/10.1002/2016JA023564

Garcia, R. G., Liberman, R., Russell, J. M., & Mlynczak, M. G. (2004). Large-scale waves in the mesosphere and lower thermosphere observed by SABER. *Journal of the Atmospheric Sciences*, *62*(12), 4384–4399. https://doi.org/10.1175/JAS3612.1

Gavrilov, N. M., & Koval, A. V. (2013). Parameterization of mesoscale stationary orographic wave forcing for use in numerical models of atmospheric dynamics. *Izvestiya Atmospheric and Ocean Physics*, *49*(3), 244–251.

Gavrilov, N. M., Koval, A. V., Pogoreltsev, A. I., & Savenkova, E. N. (2015). Simulating influences of QBO phases and orographic gravity wave forcing on planetary waves in the middle atmosphere. *Earth, Planets and Space*, *67*(1), 86. https://doi.org/10.1186/s40623-015-0259-2

Gavrilov, N. M., Pogoreltsev, A. I., & Jacobi, C. (2005). Numerical modeling of the effect of latitude-inhomogeneous gravity waves on the circulation of the middle atmosphere. *Izvestiya, Atmospheric and Oceanic Physics*, *41*(1), 9–18.

Geller, M. A., & Alpert, J. C. (1980). Planetary wave coupling between the troposphere and the middle atmosphere as a possible Sun-weather mechanism. *Journal of the Atmospheric Sciences*, *37*(6), 1197–1215. https://doi.org/10.1175/1520-0469(1980)037<1197:PWCBTT>2.0.CO;2

Gray, L. J., Sparrow, S., Juckes, M., O'Neill, A., & Andrews, D. G. (2003). Flow regime in the winter stratosphere of the Northern Hemisphere. *Quarterly Journal of the Royal Meteorological Society*, *129*(589), 925–945. https://doi.org/10.1256/qj.02.82

Gu, S. Y., Liu, H. L., Li, T., Dou, T. X., Wu, Q., & Russell, J. M. III (2014). Observation of the neutral-ion coupling through 6 day planetary wave. *Journal of Geophysical Research: Space Physics*, *119*, 10,376–10,383. https://doi.org/10.1002/2014JA020530

Gulyaeva, T. L., Huang, X., & Reinisch, B. W. (2002). Ionosphere-plasmasphere model software for ISO. *Acta Geodaetica et Geophysica Hungarica*, *37*(2–3), 143–152. https://doi.org/10.1556/AGeod.37.2002.2-3.3

Hoffmann, P., & Jacobi, Ch. (2006). Analysis of planetary waves seen in ionospheric total electron content (TEC) perturbations. *Wiss. Mitteil*. Inst. f. Meteorol. Univ. Leipzig Band 37.

Holton, J. R. (1975). The dynamic meteorology of the stratosphere and mesosphere. *Meteorological Monographs*, *15*(37), 218.

Holton, J. R., & Mass, C. (1976). Stratospheric vacillation cycles. *Journal of the Atmospheric Sciences*, *33*(11), 2218–2225. https://doi.org/10.1175/1520-0469(1976)033<2218:SVC>2.0.CO;2

Hoppner, K., & Bittner, M. (2007). Evidence for solar signals in the mesopause temperature variability? *Journal of Atmospheric and Solar - Terrestrial Physics*, *69*(4-5), 431–448. https://doi.org/10.1016/j.jastp.2006.10.007

Jacobi, C., Hoffmann, P., & Kurschner, D. (2008). Trends in MLT region winds and planetary waves, Collm (52°N, 15°E). *Annales Geophysicae*, *26*(5), 1221–1232. https://doi.org/10.5194/angeo-26-1221-2008

Karoly, D. J., & Hoskins, B. J. (1982). Three dimensional propagation of planetary waves. *Journal of the Meteorological Society of Japan*, *60*, 109–123.

Kobayashi, S., Ota, Y., & Harada, H. (2015). The JRA-55 reanalysis: General specifications and basic characteristics. *Journal of the Meteorological Society of Japan*, *93*(1), 5–48. https://doi.org/10.2151/jmsj.2015-00

Koval, A. V., Gavrilov, N. M., Pogoreltsev, A. I., & Shevchuk, N. O. (2018). Propagation of stationary planetary waves to the thermosphere at different levels of solar activity. *Journal of Atmospheric and Solar - Terrestrial Physics*, *173*, 140–149. https://doi.org/10.1016/j.jastp.2018.03.012

Krivolutsky, A. A., Cherepanova, L. A., Dement'eva, A. V., Repnev, A. I., & Klyuchnikova, A. V. (2015). Global circulation of the Earth's atmosphere at altitudes from 0 to 135 km simulated with the ARM model. Consideration of the solar activity contribution. *Geomagnetism and Aeronomy*, *55*(6), 780–800. https://doi.org/10.1134/S0016793215060067

Laštovicka, J. (2006). Forcing of the ionosphere by waves from below. *Journal of Atmospheric and Solar - Terrestrial Physics*, *68*(3-5), 479–497. https://doi.org/10.1016/j.jastp.2005.01.018

Lindzen, R. S. (1981). Turbulence and stress owing to gravity wave and tidal breakdown. *Journal of Geophysical Research*, *86*, 9707–9714.

Liu, H. -L., Bardeen, C. G., Foster, B. T., Lauritzen, P., Liu, J., Lu, G., & Wang, W. (2018). Development and validation of the whole atmosphere community climate model with thermosphere and ionosphere extension (WACCM-X 2.0). *Journal of Advances in Modeling Earth Systems*, *10*(2), 381–402. https://doi.org/10.1002/2017MS001232

Liu, H. -L., & Richmond, A. D. (2013). Attribution of ionospheric vertical plasma drift perturbations to large-scale waves and the dependence on solar activity. *Journal of Geophysical Research: Space Physics*, *118*, 2452–2465. https://doi.org/10.1002/jgra.50265

Liu, H. L., Talaat, E. R., Roble, R. G., Lieberman, R. S., Riggin, D. M., & Yee, J. H. (2004). The 6.5-day wave and its seasonal variability in the middle and upper atmosphere. *Journal of Geophysical Research*, *109*, D21112. https://doi.org/10.1029/2004JD004795

Liu, X., Xu, J., Zhang, S., Jiang, G., Zhou, Q., Yuan, W., et al. (2014). Thermospheric planetary wave-type oscillations observed by FPIs over Xinglong and Millstone Hill. *Journal of Geophysical Research: Space Physics*, *119*, 6891–6901. https://doi.org/10.1002/2014JA020043

Longuet-Higgins, M. S. (1968). The eigenfunctions of Laplace's tidal equation over a sphere. *Philosophical Transactions of the Royal Society of London*, *262*(1132), 511–607. https://doi.org/10.1098/rsta.1968.0003

Lopez-Gonzalez, M. J., Rodrıguez, E., Garcıa-Comas, M., Costa, V., Shepherd, M. G., Shepherd, G. G., et al. (2009). Climatology of planetary wave type oscillations with periods of 2–20 days derived from O2 atmospheric and OH(6-2) airglow observations at mid-latitude with SATI. *Annales de Geophysique*, *27*(9), 3645–3662. https://doi.org/10.5194/angeo-27-3645-2009

Lu, H., Scaife, A. A., Marshall, G. J., Turner, J., & Gray, L. J. (2017). Downward wave reflection as a mechanism for the stratosphere-troposphere response to the 11-year solar cycle. *Journal of Climate*, *30*(7), 2395–2414. https://doi.org/10.1175/JCLI-D-16-0400.1

Matsuno, T. (1966). Numerical integration of the primitive equations by a simulated backward difference method. *Journal of the Meteorological Society of Japan*, *44*(1), 76–84. https://doi.org/10.2151/jmsj1965.44.1_76

Matsuno, T. (1970). Vertical propagation of stationary planetary waves in the winter northern hemisphere. *Journal of the Atmospheric Sciences*, *27*(6), 871–883. https://doi.org/10.1175/1520-0469(1970)027<0871:VPOSPW>2.0.CO;2

Meyer, C. K. (1999). Gravity wave interactions with mesospheric planetary waves: A mechanism for penetration into the thermosphere-ionosphere system. *Journal of Geophysical Research*, *104*, 28,181–28,196. https://doi.org/10.1029/1999JA900346

Mitchell, N. J., Middleton, H. R., Beard, A. G., Williams, P. J. S., & Muller, H. G. (1999). The 16-day planetary wave in the mesosphere and lower thermosphere. *Annales de Geophysique*, *17*(11), 1447–1456. https://doi.org/10.1007/s00585-999-1447-9

Pancheva, D., Alberca, L. F., & Morena, B. A. (1994). Simultaneous observations of quasi-two-day variations in the lower and upper ionosphere over Europe. *Journal of Atmospheric and Solar - Terrestrial Physics*, *56*(1), 43–50. https://doi.org/10.1016/0021-9169(94)90174-0

Pancheva, D., & Mukhtarov, P. (2012). Planetary wave coupling of the atmosphere–ionosphere system during the northern winter of 2008/2009. *Advances in Space Research*, *50*(9), 1189–1203.

Pancheva, D., Mukhtarov, P., Andonov, B., & Forbes, J. M. (2010). Global distribution and climatological features of the 5-6-day planetary waves seen in the SABER/TIMED temperatures (2002-2007). *Journal of Atmospheric and Solar - Terrestrial Physics*, *72*(I. 1), 26–37.

Pedatella, N. M., & Forbes, J. M. (2009). Modulation of the equatorial F-region by the quasi-16-day planetary wave. *Geophysical Research Letters*, *36*, L09105. https://doi.org/10.1029/2009GL037809

Picone, J. M., Hedin, A. E., Drob, D. P., & Aikin, A. C. (2002). NRLMSISE-00 empirical model of the atmosphere: Statistical comparisons and scientific issues. *Journal of Geophysical Research*, *107*(A12), 1468. https://doi.org/10.1029/2002JA009430

Pogoreltsev, A. I. (1996). Production of electromagnetic field disturbances due to the interaction between acoustic gravity waves and the ionospheric plasma. *Journal of Atmospheric and Solar - Terrestrial Physics*, *58*(10), 1125–1141.

Pogoreltsev, A. I. (1999). Simulation of planetary waves and their influence on the zonally averaged circulation in the middle atmosphere. *Earth, Planets and Space*, *51*(7-8), 773–784. https://doi.org/10.1186/BF03353236

Pogoreltsev, A. I. (2007). Generation of normal atmospheric modes by stratospheric vacillations. *Izvestiya Atmospheric and Oceanic Physics*, *43*(4), 423–435.

Pogoreltsev, A. I., Kanukhina, A. Y., Suvorova, E. V., & Savenkova, E. N. (2009). Variability of planetary waves as a signature of possible climatic changes. *Journal of Atmospheric and Solar - Terrestrial Physics*, *71*(14-15), 1529–1539. https://doi.org/10.1016/j.jastp.2009.05.011

Pogoreltsev, A. I., Savenkova, E. N., & Pertsev, N. N. (2014). Sudden stratopheric warmings: The role of normal atmospheric modes. *Geomagnetism and Aeronomy*, *54*(2), 1–15.

Pogoreltsev, A. I., Vlasov, A. A., Fröhlich, K., & Jacobi, C. (2007). Planetary waves in coupling the lower and upper atmosphere. *Journal of Atmospheric and Solar - Terrestrial Physics*, *69*(17-18), 2083–2101. https://doi.org/10.1016/j.jastp.2007.05.014

Qian, L., Burns, A. G., Emery, B. A., Foster, B., Lu, G., Maute, A., et al. (2013). The NCAR TIE-GCM: A community model of the coupled thermosphere/ionosphere system. *Geophysical Monograph Series*, *201*, 73–83.

Rice, J. A. (2006). *Mathematical statistics and data analysis* (3rd ed., p. 603). Pacific Grove: Duxbury Press.

Richards, P. G., Fennelly, J. A., & Torr, D. G. (1994). EUVAC: A solar EUV flux model for aeronomic calculations. *Journal of Geophysical Research*, *99*, 8981–8992.

Riggin, D. M., Liu, H. -L., Lieberman, R. S., Roble, R. G., Russell, J. M. III, Mertens, C. J., et al. (2006). Observations of the 5-day wave in the mesosphere and lower thermosphere. *Journal of Atmospheric and Solar - Terrestrial Physics*, *68*(I. 3-5), 323–339.

Royal Observatory of Belgium (ROB) (2013). Retrieved from http://sidc.be/silso/datafiles

Shevchuk, N. O., Ortikov, M. Y., & Pogoreltsev, A. I. (2018). Modeling of atmospheric tides with account of diurnal variations of Ionospheric conductivity. *Russian Journal of Physical Chemistry B*, *12*(3), 576–589. https://doi.org/10.1134/S199079311803017X

Smith, A. K. (2003). The origin of stationary planetary waves in the upper mesosphere. *Journal of the Atmospheric Sciences*, *60*(24), 3033–3041. https://doi.org/10.1175/1520-0469(2003)060<3033:TOOSPW>2.0.CO;2

Strang, G. (1968). On the construction and comparison of difference schemes. *SIAM Journal on Numerical Analysis*, *5*, 516–517.

Stray, N. H., & Espy, P. J. (2018). Planetary wave-like oscillations in the ionosphere retrieved with a longitudinal chain of ionosondes at high northern latitudes. *Journal of Atmospheric and Solar - Terrestrial Physics*, *171*, 225–233. https://doi.org/10.1016/j.jastp.2017.10.011

Suvorova, E. V., & Pogoreltsev, A. I. (2011). Modeling of nonmigrating tides in the middle atmosphere. *Geomagtetism and Aeronomy*, *51*(1), 105–115. https://doi.org/10.1134/S0016793210061039

Swarztrauber, P. N., & Kasahara, A. (1985). The vector harmonic analysis of Laplace's tidal equations. *SIAM Journal on Scientific and Statistical Computing*, *6*(2), 464–491. https://doi.org/10.1137/0906033

Takahashi, H., Lima, L. M., Wrasse, C. M., Abdu, M. A., Batista, I. S., Gobbi, D., et al. (2005). Evidence on 2–4 day oscillations of the equatorial ionosphere h0F and mesospheric airglow emission. *Geophysical Research Letters*, *32*, L12102. https://doi.org/10.1029/2004GL022318

Takahashi, H., Wrasse, C. M., Fechine, J., Pancheva, D., Abdu, M. A., Batista, I. S., et al. (2007). Signatures of ultra fast Kelvin waves in the equatorial middle atmosphere and ionosphere. *Geophysical Research Letters*, *34*, L11108. https://doi.org/10.1029/2007GL029612

Tapping, K. F. (1987). Recent solar radio astronomy at centimeter wavelength: The temporal variability of the 10.7-cm flux. *Journal of Geophysical Research*, *92*(D1), 829–838.

Wang, J. C., Chang, L. C., Yue, J., Wang, W., & Siskind, D. E. (2017). The quasi 2 day wave response in TIME-GCM nudged with NOGAPS-ALPHA. *Journal of Geophysical Research: Space Physics*, *122*, 5709–5732. https://doi.org/10.1002/2016JA023745

Yamazaki, Y., & Richmond, A. D. (2013). A theory of ionospheric response to upward-propagating tides: Electrodynamic effects and tidal mixing effects. *Journal of Geophysical Research: Space Physics*, *118*, 5891–5905. https://doi.org/10.1002/jgra.50487

Yigit, E., & Medvedev, A. S. (2009). Heating and cooling of the thermo-sphere by internal gravity waves. *Geophysical Research Letters*, *36*, L14807. https://doi.org/10.1029/2009GL038507

Yoden, S. (1990). An illustrative model of seasonal and interannual variations of the stratospheric circulation. *Journal of the Atmospheric Sciences*, *47*(15), 1845–1853. https://doi.org/10.1175/1520-0469(1990)047<1845:AIMOSA>2.0.CO;2

Zaragoza, G., & Taylor, F. W. (2001). Latitudinal and longitudinal behavior of the mesospheric OH nightglow layer as observed by the improved stratospheric and mesospheric sounder on UARS. *Journal of Geophysical Research*, *106*(D8), 8027–8033. https://doi.org/10.1029/2000JD900633

Zhu, Z., Luo, W., Lan, J., & Chang, S. (2017). Features of 3–7-day planetary-wave-type oscillations in *F*-layer vertical drift and equatorial spread F observed over two low-latitude stations in China. *Annales de Geophysique*, *35*(3), 763–776. https://doi.org/10.5194/angeo-35-763-2017